Journal Pre-proofs

Development and evaluation of an exoskeleton-assisted upper limb telerehabilitation system based on multi-sensor information fusion

He Li, Shuxiang Guo, Ruijie He, Bin Wang, Mingchao Ding

PII: S0263-2241(26)01029-8
DOI: https://doi.org/10.1016/j.measurement.2026.121320
Reference: MEASUR 121320

To appear in: *Measurement*

Received Date: 25 November 2025
Revised Date: 14 February 2026
Accepted Date: 26 March 2026

Please cite this article as: H. Li, S. Guo, R. He, B. Wang, M. Ding, Development and evaluation of an exoskeleton-assisted upper limb telerehabilitation system based on multi-sensor information fusion, *Measurement* (2026), doi: https://doi.org/10.1016/j.measurement.2026.121320

Development and Evaluation of an Exoskeleton-assisted Upper Limb Telerehabilitation System based on Multi-sensor Information Fusion

He Li[1, 2, 3, 4*], Shuxiang Guo[4, 5, 6*], Ruijie He[4], Bin Wang[6], Mingchao Ding[6]

[1.] First Teaching Hospital of Tianjin University of Traditional Chinese Medicine, Tianjin 300381, China.
[2.] National Clinical Research Center for Chinese Medicine, Tianjin 300381, China.
[3.] Tianjin Key Laboratory of Acupuncture and Moxibustion, Tianjin 300381, China.
[4.] Key Laboratory of Convergence Biomedical Engineering System and Healthcare Technology, The Ministry of Industry and Information Technology, Beijing Institute of Technology, Beijing 100081, China.
[5.] Department of Electronic and Electrical Engineering, Southern University of Science and Technology, Shenzhen, Guangdong 518055, China.
[6.] Department of Peripheral Vascular Intervention, Aerospace Center Hospital, School of Life Science, Beijing Institute of Technology, Beijing 100081, China.

Corresponding author e-mail: 15930779203@163.com (He Li)
guo.shuxiang@sustech.edu.cn (Shuxiang Guo)

With the increasing number of patients with upper limb hemiplegia, robot-assisted rehabilitation has attracted increasing attention. Compared with traditional face-to-face training, telerehabilitation with therapist-in-the-loop is an effective alternative. During the telerehabilitation training, the complementary assessment methods are essential, which form the basis for formulating rehabilitation treatment plans. However, at present, most assessments are either subjective evaluations by physicians or objective methods that cannot be combined with robots, which are not suitable for the telerehabilitation training based on upper limb exoskeleton. This paper builds an exoskeleton-assisted upper limb telerehabilitation system leveraging a cloud server. Based on the telerehabilitation system, an assessment method using multi-sensor information fusion is proposed. Experiments were conducted involving passive movements (simulating complete hemiplegia) and active movements (simulating no hemiplegia). Further, data preprocessing and data derivation were carried out. Finally, the collected multi-sensor data were fused through machine learning algorithms to achieve the classification of different rehabilitation states. Although the method proposed in this study is designed for simplified scenarios, it has the potential to develop assessment methods compatible with rehabilitation exoskeleton.

Key words: Rehabilitation Assessment, Telerehabilitation, Exoskeleton, Surface Electromyography (sEMG), Force Myography (FMG), Human-robot Interaction Force (HRIF)

I. INTRODUCTION

Stroke is a leading cause of hemiplegia, with 40–60% resulting in motor deficits in one of the upper extremities [1]. Upper limb hemiplegia affects patients' daily life and significantly reduces their quality of life. Timely and effective rehabilitation training can reduce motor impairment and restore the motor function of hemiplegia patients' affected side [2]. Therefore, rehabilitation treatment is essential for the patients.

However, rehabilitation care is a long-term process. On the one hand, this will bring a substantial psychological and financial burden to the families. On the other hand, the demand for stroke rehabilitation services is growing [3], and the increasing number of stroke survivors creates a greater need for rehabilitation services. Due to the lack of rehabilitation institutes and therapists, only a small number of stroke survivors have access to professional rehabilitation training. In other words, traditional rehabilitation training brings a heavy burden for both the family and the healthcare system. Robotic rehabilitation opens up a new avenue for stroke rehabilitation [4]-[6]. Compared to conventional rehabilitation, robots used in rehabilitation are practical and cost-effective. They can quantitatively assess the effects of rehabilitation and provide training consistently and repetitively, which frees therapists from repetitive and tedious work. Therefore, rehabilitation robots are expected to be essential in future rehabilitation treatment [7]-[9].

Compared to traditional rehabilitation training that requires face-to-face interaction with a therapist, the telerehabilitation [10] assisted by robots can pair rehabilitation robots with information technology and transfer evaluation data over the internet to the therapist. Therefore, treatment can be transferred from one specialized facility to the patients' home and supervised remotely by a therapist.

At the same time, it can reduce the cost of treatment, the time spent on the way to the clinic, and the economic burden on patients. Rehabilitation assessment is not only the basis for formulating rehabilitation treatment programs but also the objective standard for observing the therapeutic effect, which plays an important role in the telerehabilitation treatment, evaluation of therapeutic effect, and prediction of functional recovery [11]. At present, there are two kinds of assessment methods: subjective evaluation and objective evaluation [12]. In the subjective assessment, the motor function of stroke survivors and the effect of therapeutic intervention are usually assessed by therapists using clinical assessment scales, such as the Brunnstrom assessment method and the Fugl-Meyer assessment scale. These are subjective assessment methods employed by rehabilitation physicians. To improve the function of the rehabilitation training robot and realize the quantitative evaluation of the upper limb motor function of hemiplegia patients, it is necessary to establish a well rehabilitation quantitative evaluation system and implement quantitative evaluation and training tracking functions for rehabilitation patients. Then the standardized and quantitative development of rehabilitation training process can be realized.

Objective evaluation mostly focuses on bioelectrical signals to carry out rehabilitation assessment studies, such as using Surface Electromyography (sEMG), Force Myography (FMG), Electroencephalogram (EEG), and other relevant features to conduct rehabilitation assessment of patients. Zhang et al. designed a rehabilitation training system based on EEG and EMG signals and studied the evaluation methods of motor function in the rehabilitation process, which can provide reference for automatic and objective rehabilitation assessment methods [13]. Bai et al. proposed a method to evaluate upper limb motor function in stroke patients using the relative surface area of the envelope of the upper limb's accessible workspace [14]. Lu et al. applied unsupervised feature learning techniques to reduce the complexity of building the evaluation model of patients' progress [15]. Grimm et al. compared their sensor-based assessment with the clinical outcome based on one commercial rehabilitation exoskeleton [16]. Ding et al. proposed a novel quantitative evaluation system based on force feedback and machine learning algorithm [17]. Although the aforementioned studies have carried out a series of studies on rehabilitation evaluation, they have not been effectively combined with upper limb rehabilitation exoskeleton, particularly for home-based telerehabilitation.

Furthermore, beyond assessment alone, the ultimate goal of rehabilitation robots is to achieve seamless and adaptive cooperative control with the patient. Recent studies have explored this direction by integrating multimodal wearable training evaluation with human-exoskeleton cooperative control strategies. For instance, Zhao et al. have proposed a multilevel control strategy for human-exoskeleton cooperative motion with integrated wearable training evaluation [18], while Kou et al. have investigated gait planning and multimodal cooperative control based on central pattern generators [19]. These works underscore the trend towards intelligent control systems that utilize real-time physiological and biomechanical data to adjust assistance. However, a foundational prerequisite for such adaptive control in telerehabilitation is a robust, objective, and multi-sensor-based assessment method that can accurately and remotely identify the patient's motor state. Therefore, this paper proposes a rehabilitation assessment method based on our self-developed portable upper limb exoskeleton, which is equipped with multi-source sensors.

In this paper, an objective assessment method of exoskeleton-assisted upper limb rehabilitation based on multi-sensor information fusion is proposed for the therapist-in-the-loop telerehabilitation. In telerehabilitation training, one therapist operates the haptic device to control the exoskeleton to drive the movements of patient's affected side. At the same time, the data of sEMG, FMG, and human-robot interaction force (HRIF) of the affected side are collected. The data collection is carried out in two situations: (1) passive movements - the affected side is completely driven by the exoskeleton; (2) active movements - the affected side follows the corresponding movements of the exoskeleton, and the data collection of multi-source sensors is completed in the above two situations respectively. Then, through data derivation, the above two rehabilitation states are refined into four categories: (1) complete hemiplegia, (2) severe hemiplegia, (3) mild hemiplegia, and (4) no hemiplegia. Finally, the multi-sensor information fusion is realized to complete the classification of four types of states through machine learning algorithms, that is, the current rehabilitation process of patients can be evaluated.

The rest of the paper is organized as follows. Section II describes the hardware description, which includes the overview of the telerehabilitation system, the portable upper limb exoskeleton, and the multi-source sensors. The introduction of the multi-sensor fusion in this study is described in Section III. In Section IV, the experiments are shown. Section V is the conclusion.

II. Hardware Description

The exoskeleton system developed herein is designed for assessment-oriented telerehabilitation of hemiplegia patients. Its design is distinguished by three principal innovations: (1) seamless integration into a remote supervisory platform that is cloud-based and incorporates a therapist-in-the-loop; (2) an anatomically adaptive forearm mechanism employing a rail-slider and spring to compensate for variations in joint mobility and improve operational safety; and (3) integrated multimodal sensing (sEMG, FMG, HRIF) to facilitate real-time neuromuscular assessment during assistive operation. The subsequent subsections elaborate on the hardware implementation.

A. Overview of the Telerehabilitation System

Figure 1 shows the schematic diagram of the telerehabilitation system. This system includes the therapist side and the robot-assisted limb side. One user (serves as a therapist) operates the haptic device HD^2 (Quanser, Canada) on the master side, and another user (serves as a patient with upper limb hemiplegia) wears the upper limb rehabilitation exoskeleton. The motion signal is transmitted from the therapist side to the robot-assisted side, and the HRIF between the exoskeleton and the subject is transmitted from the robot-assisted side to the therapist side synchronously. This bidirectional interaction enables the system to operate in a therapist-in-the-loop control mode, where the therapist can sense the interaction forces and adapt the movement intuitively, introducing human adaptability into the control loop. During the telerehabilitation training, motion angles, sEMG and FMG signals, and the HRIF signals are recorded, which will be used for rehabilitation assessment.

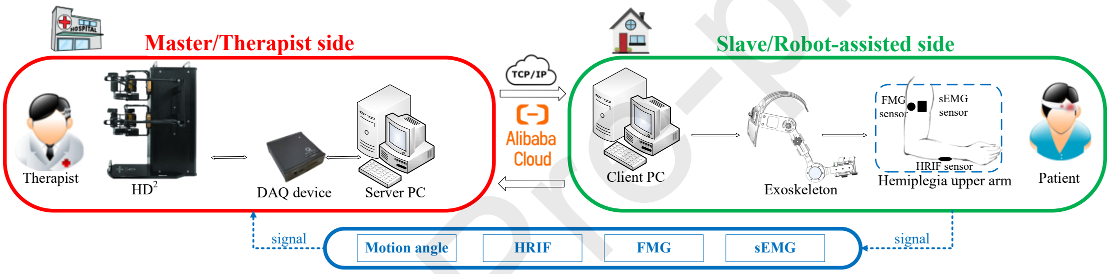

Legend:
FMG: Force Myography; **sEMG**: Surface Electromyography; **HRIF**: Human-robot Interaction Force; **HD^2**: High Definition Haptic Device;
TCP/IP: Transmission Control Protocol/Internet Protocol; **DAQ:** Data Acquisition;

Figure 1. Overview of the telerehabilitation system

B. Cloud Server-based Communication

The operating environment of HD^2 is developed in the MATLAB & Simulink (2022b, MathWorks, United States), so the telerehabilitation system involved in this study is also based on the MATLAB & Simulink. Considering the connection stability and implementation complexity, the signal transmission of the telerehabilitation system adopts a socket communication mechanism and TCP protocol in this preliminary exploration of cloud-based teleoperation. A socket consists of an IP address and a port number to identify each separate data stream uniquely. Ali Cloud is chosen as the cloud platform with the Windows Server 2012 R2 system, for both the master PC and the slave PC. Therefore, intranet penetration is required between the cloud server and the master computer. Fast Reverse Proxy (FRP) is adopted in this study to implement intranet penetration. The port mapping diagram is shown in Figure 2.

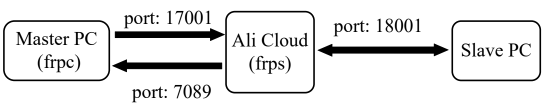

Figure 2. Port mapping in TCP intranet penetration

Based on the TCP intranet penetration and the GNSS clock synchronization, the communication model in Simulink is built, as shown in Figure 3 (a) and (b). This Simulink model includes the master side and the slave side. The communication module of the master side uses the "Stream Server" module in QuaRC, and the communication module of the slave side uses the "TCP Client" module. Timestamps were added to both sides to calculate the communication delay between master

PC and slave PC, respectively. In the slave computer, the "MATLAB function" module is adopted to obtain PC time. In the master computer, the "Data/time" module of QuaRC is adopted to get the PC time.

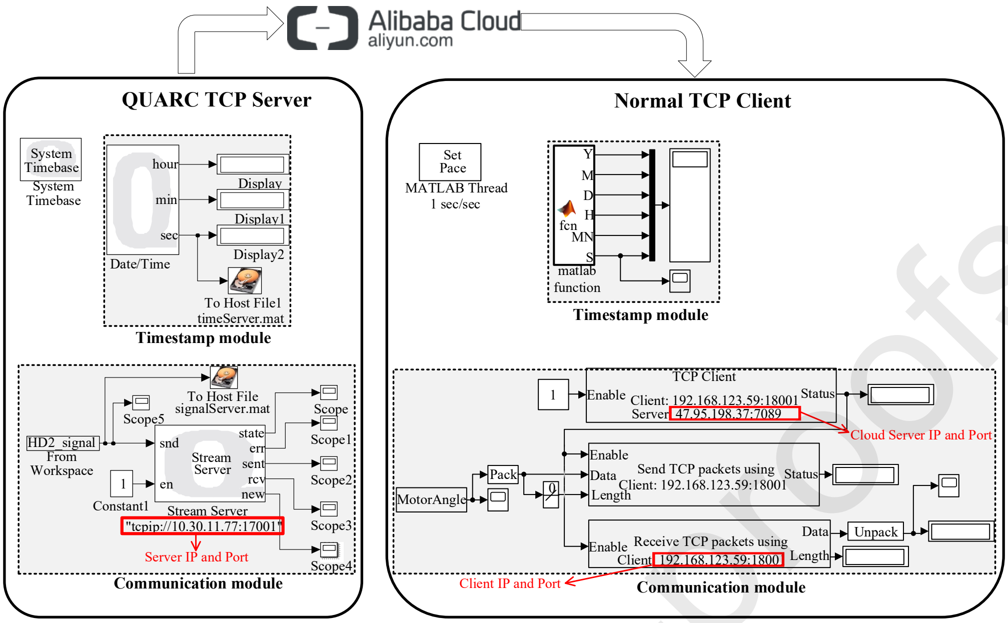

(a) (b)

Figure 3. Communication module (a) master communication module in Simulink (b) slave communication module in Simulink

For the telerehabilitation system, the time delay and angle error are evaluated. Mean Absolute Error (MAE), Root Mean Square Error (RMSE), and Correlation Coefficient (R) are adopted to evaluate the angle error. MAE (as shown in (1)) is the average of all absolute errors between the target and true angles. RMSE (as shown in (2)) is the standard deviation of the target and true angles. R (as shown in (3)) is a number between -1 and 1 that tells the correlation between the target and true angles.

$$MAE = \frac{1}{N}\sum_{i=1}^{N}(y_i - x_i) \tag{1}$$

$$RMSE = \sqrt{\frac{1}{N}\sum_{i=1}^{N}(y_i - x_i)^2} \tag{2}$$

$$R = \frac{\sum_{i=1}^{N}(x_i - \overline{x})(y_i - \overline{y})}{\sqrt{\sum_{i=1}^{N}(x_i - \overline{x})^2 \sum_{i=1}^{N}(y_i - \overline{y})^2}} \tag{3}$$

where x_i represents the master side's motion angles at the ith data point, $\bar{x}$ is the average value, y_i means the slave side's motion angles at the ith data point, $\bar{y}$ is the average value, and N is the total number of data points.

C. Portable Upper Limb Exoskeleton

The diagram of the upper limb exoskeleton is shown in Figure 4, in which (a) shows the bone structure of the elbow joint. Figure 4 (b) shows the Solidworks (2021, Dassault Systemes S.A., United States) model of the upper limb rehabilitation exoskeleton, which includes 3 passive degrees of freedom (DOFs) and 1 active DOF. The distance between the humerus and the radius increases during elbow extension, whereas the distance decreases during elbow flexion. To accommodate this distance variation, a structure combining a rail and a slider is designed for the exoskeleton forearm, as shown in the red dotted box of Figure 4 (b). The spring in this structure provides restoring force, and a green silicone pad at its end acts as a cushion.

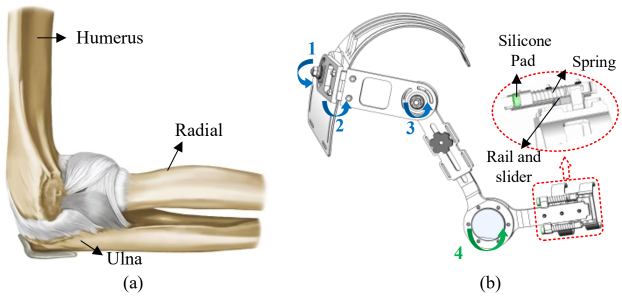

Figure 4. Diagram of the elbow joint and exoskeleton. (a) the bone structure of the elbow joint (b) the Solidworks model of the upper limb exoskeleton

The upper limb exoskeleton worn by one subject is shown in Figure 5. Its mechanical structure mainly contains three parts: shoulder part, upper arm part, and forearm part. The shoulder part includes the shoulder backplate and the junction plate. The shoulder backplate is attached to the body by two fabric straps. The junction plate is connected via a hinge to increase one DOF at the shoulder. These passive DOFs are designed to improve wearable comfort and align with natural joint kinematics, thereby reducing unwanted constraints and mechanical impedance. The length of the upper arm and the forearm can be adjusted according to the arm length of different subjects. The upper arm of the exoskeleton is immobilized with a rehabilitation shoulder pad (aiwecare, Taiwan, China). The elbow joint rotation is realized through a brushless joint motor (AK 60-6, CubeMars, China). The power module integrates a high-performance brushless motor, a planetary reducer and encoder, and an integrated drive, which can achieve high torque and smooth operation. The motor uses a portable drive scheme, supports two control modes of servo operation and control, enables synchronous control of position, speed, and acceleration beyond conventional schemes

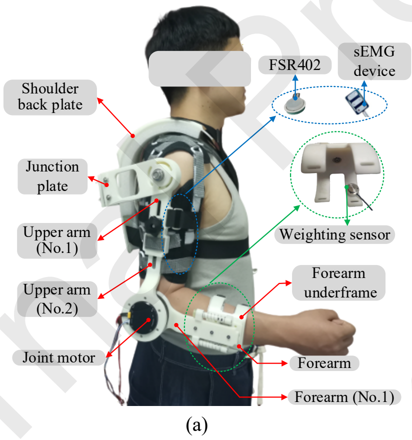

Figure 5. The upper limb exoskeleton worn by one subject. (a) lateral view (b) front view

The embedded system includes high-level and low-level control, as shown in Figure 6. The high-level control is implemented in MATLAB & Simulink, including modules for HD^2 angle acquisition and remote data transmission. The HD^2 system is connected to the computer via Quanser's superior hardware control board QID/QIDe, using its Real-Time Control (QuaRC) software compatible with MATLAB & Simulink. The low-level motor control is realized in Arduino Mega 2560, which adopts the position-speed loop mode in the servo mode. In this mode, the position, speed, and acceleration of motor are specified, and the motor will run to the specified position with the given acceleration and maximum speed.

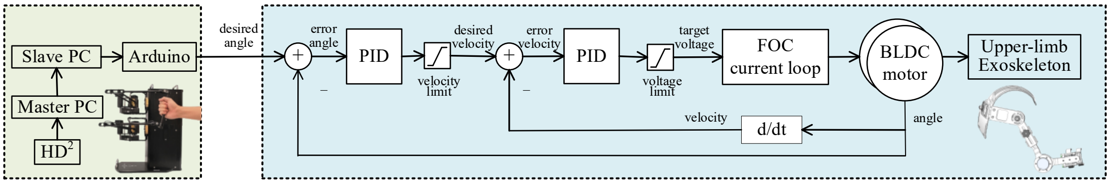

Figure 6. The embedded system of the motor control

D. Multi-source Sensors

A dry-electrode sEMG sensor, which integrates filtering and amplifying circuits (amplifying weak sEMG signals within ± 1.5 mV by 1000 times), effectively suppresses noise (especially power frequency interference) through differential input and analog filtering circuits. This sensor collects analog signals, which can be sampled by Arduino. It is placed on the biceps of the affected side to acquire sEMG signals, as shown in Figure 5 (a). The CYMH-1 (ChengYing, China) is a micro planar weighing sensor, which is suitable for use on occasions with limited space and is more stable compared with sensors based on thin-film resistor sensors. This sensor collects analog signals, which can also be sampled by Arduino. This weighting sensor device is placed on the forearm underframe to collect HRIF signals, as shown in Figure 5 (a). This signal is not only used for rehabilitation assessment but also provides a real-time safety monitoring channel that can detect abnormal resistance, such as spasticity, potentially triggering safety protocols in future clinical implementations.

The FSR402 shown in Figure 7 (a) is a lightweight, compact, highly accurate, and ultra-thin resistive pressure sensor manufactured by Interlink Electronics. This pressure sensor converts the pressure applied to the thin film region of the sensor into a change in the resistance value to obtain pressure information. The higher the pressure, the lower the resistance. It is allowed to be used within a pressure range of 100 g to 10 kg, which is within the range of the force generated by a contracted muscle pressing into the sensor. As one of the most popular and affordable FMG sensors [20], FSR402 is used in this study to acquire FMG signals. The formula between the output voltage and the applied pressure is shown in (4).

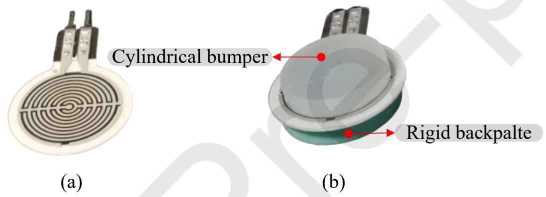

Figure 7. The FSR402 in two configurations. (a) without modifications (b) with modifications

$$U_0 = \frac{3.2}{F_{max}} \times F + 0.1 \tag{4}$$

where U_0 is the output voltage of the conversion module, F is the pressure value.

Figure 7 (a) and (b) show the unmodified sensor and modified version of the sensor. The modified version is coupled with a self-made backplate and bumper. By adding a rigid backplate between the sensor and armband (part of the shoulder pad and used to fix the sEMG module and the FSR402 sensor), axial forces generated by the volumetric changes associated with muscle contraction are concentrated onto the sensor. Further, using a bumper on the force-sensing region helps to concentrate the force generated onto the sensing membrane. This sensor collects analog signals, which can also be sampled by Arduino. It is also placed on the biceps of the affected side, as shown in Figure 5 (a).

III. Multi-sensor Fusion

A. Data Preprocessing

To utilize the data from multi-source sensors, preprocessing and interpolation are necessary. The main energy distribution of sEMG signals is in the range of 20 to 150 Hz. According to the Nyquist Sampling Theorem, the minimum sampling frequency for sEMG signals is 300 Hz. Here, the sampling frequency of the single-channel dry electrode is set to 500 Hz, which is also the sampling frequency of FMG signals.

Signal preprocessing is an important step. The raw signal is relatively weak and greatly affected by noise and interference, which can adversely affect the signal analysis. Therefore, the pre-processing of the signal is important, which can improve the signal quality and make the subsequent signal analysis and processing more accurate and reliable. The high-pass filter at 20 Hz is used to eliminate the low-frequency noise, and a notch filter at 50 Hz is used to remove power frequency interference. The HRIF and FMG signals are filtered by a Butterworth low-pass filter.

When processing multi-source signals, downsampling or upsampling is used to synchronize multiple signals to the same sampling rate. The sampling frequency of sEMG, HRIF, and FMG are all 500 Hz. However, the motor signal is only sampled at 50 Hz, thus the motor angle data are upsampled to 500 Hz by a factor of 10 to match the sampling rate of other sensor data.

B. Sliding Window and Feature Extraction

After filtering, because sEMG is highly non-stationary, the data should then be segmented into time series to maintain signal stability. The sliding window is adopted in this study. Windowing is crucial for further signal processing, as it is used to extract the underlying signal features. The optimal windowing procedure is a trade-off between window size and overlap between adjacent windows. The length of the window is proportional to the classification accuracy, that is, the longer the window, the higher the classification accuracy. However, as the window length increases, the latency increases. Therefore, the overlapping windowing can be used for larger window lengths to decrease the time delay [21]. This approach can increase the number of samples. Figure 8 is the schematic diagram of the time window segmentation process. The sliding window is 250 ms, with an overlap of 200 ms, which meets the requirement of real-time control with a latency of less than 300 ms [22]. The data of the multi-sensor signals are all processed according to the sliding window method described above. The number of sliding windows for each subject in each time of experiments can be calculated according to (5).

$$N_{win} = \frac{1}{L_{add}}(N_{sam} - L_{win} + L_{add}) \tag{5}$$

Where, N_{win}, N_{sam}, L_{win}, L_{add} represents the number of sliding windows for each subject in each time of experiments, the number of sampling points for each subject in each time of experiments, the window length, and the window increment, respectively.

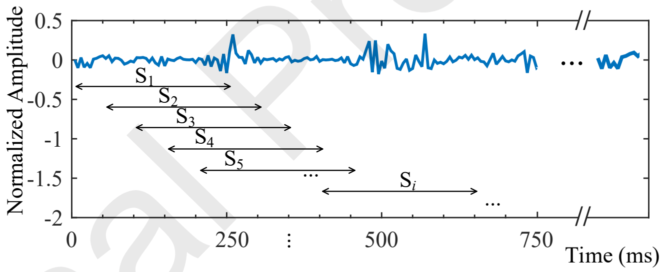

Figure 8. Schematic diagram of the sliding window method on sEMG signals. S_i represents the ith segment of sEMG signal

After the windows have been segmented, the window-based features should then be calculated. Features can be categorized into time-domain, frequency-domain, and time-frequency-domain. Time-domain features can reflect the strength of muscle contraction, and their extraction is typically less computationally expensive. Hence, time-domain features are adopted in this paper, including Mean Absolute Value (MAV), Root Mean Square (RMS), Maximum (MAX) and Minimum (MIN), respectively. MAV is the average value of the signals within an analysis window, as shown in (6). RMS refers to the square root of the mean amplitude of the sEMG signal within an analysis window and is commonly used to assess the strength of muscle contraction, as shown in (7). MAX is the maximum amplitude within a window, as shown in (8). MIN is the minimum amplitude within a window, as shown in (9).

$$MAV = \frac{1}{N}\sum_{k=1}^{N}|x_k| \tag{6}$$

$$RMS = \sqrt{\frac{1}{N}\sum_{k=1}^{N}x_k^2} \tag{7}$$

$$MAX = \max_{k=1}^{N}(x_k) \tag{8}$$

$$MIN = \min_{k-1}^{N}(x_k) \tag{9}$$

where N is the sample number within a sliding analysis window, and x_k represents the kth sample within a sliding analysis window.

The features of FMG are often not used at all because they do not seem to be vital. The raw value or MAV of the signal is the most consistently successful FMG information for pattern recognition, which is likely due to the steady and high signal-to-noise ratio of FMG signals. In summary, the MAV of motion angle, FMG and HRIF are extracted, and the MAV, RMS, MAX, and MIN of the sEMG signal are extracted. Finally, a 7-dimensional feature vector is constructed.

C. Data Fusion Description

Based on the telerehabilitation system mentioned above (as shown in Figure 1), it is noted that the slave side is equipped with multiple sensors. The fusion of multi-sensor data offers several key advantages for rehabilitation state identification: (1) Improved robustness against individual physiological variability and sensor-specific noise; (2) Complementary information integration, capturing muscle activation intent (via sEMG), force generation (via FMG/HRIF), and physical human-robot interaction dynamics; (3) Enhanced classification accuracy and reliability in distinguishing rehabilitation states. Thus, different machine learning algorithms are adopted for classification to comprehensively assess the rehabilitation.

Here, the roles of various sensors are described first. For motion angle, it is related to the strength of sEMG and FMG signals, that is, the greater the maximum angle of elbow flexion, the greater the peak value of sEMG and FMG signals. For sEMG signal, it can detect the difference in electrical signals of muscle under different motion states such as flexion and extension, which also indicates that sEMG can provide a reference for clinical evaluation of follow-up treatment [23]. For FMG signal, its basic principle is similar to clinical palpation techniques that identify different limb muscles. During elbow flexion and extension, the muscles in upper arm can be felt to change differently. When the sensor is placed on upper arm, the stronger the stiffness of the musculotendinous complex, the stronger the pressure detected by the sensor. For HRIF signal, it can reflect patients' ability to exercise autonomously, and as the recovery progresses, the force magnitude typically decreases. The multi-sensor data fusion based on machine learning is realized in this paper.

In this way, when a certain sensor signal is inaccurate for one subject, the rehabilitation state can be calculated through the data of other sensors. There exists great variability among different subjects, and through multi-sensor fusion, the accurate assessment results of rehabilitation can be obtained for different subjects.

D. Application Method of Back Propagation Neural Network (BPNN) and Long Short-Term Memory (LSTM)

Following feature extraction, machine learning algorithms are then applied for classification. In this study, BPNN is adopted, which is a commonly used supervised machine learning tool and has been used in the field of sEMG-based intention recognition [24]-[26]. The network consists of three layers: the input layer, hidden layer, and output layer, where the hidden layer transmits important information between the input layer and the output layer. The neural network of BPNN is shown in Figure 9, which includes the network layer arrangement and the network structure.

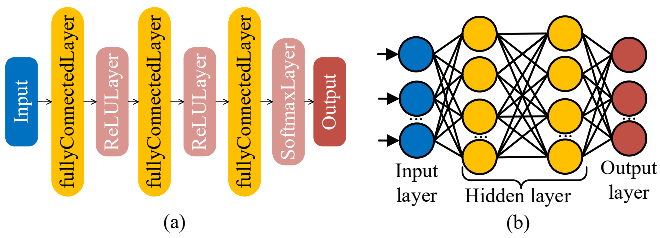

Figure 9. BP neural network (a) network layer (b) network structure

The 7-dimensional feature vectors form the input data X of BPNN and the Y represents the classification results corresponding to the four states, as shown in (10).

$$\begin{cases} X = [MAV_{angle}, MAV_{HRIF}, MAV_{FMG}, \\ \quad MAV_{sEMG}, RMS_{sEMG}, MAX_{sEMG}, MIN_{sEMG}] \\ Y = [0,1,2,3] \end{cases} \tag{10}$$

The input is the information of the multi-sensor signals, and the output is the rehabilitation grade. For the hemiplegia grade, 0 represents complete hemiplegia, 1 represents severe hemiplegia, 2 represents mild hemiplegia, and 3 represents no hemiplegia. Regarding the data splitting strategy, 5-fold cross-validation is adopted in this study.

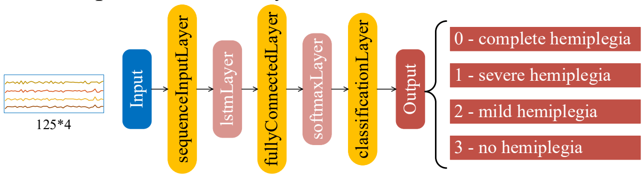

Figure 10. The network layer of LSTM.

Considering that the collected signals are time series, LSTM is further adopted. As a special variant of recurrent neural network, LSTM overcomes the modeling problem of long-term dependence by introducing a unique gating mechanism, which greatly improves the ability to learn and express time series data. The input of the LSTM network is based on the constructed sliding window (a matrix of size 125×4, where 125 is the sample number in one analysis window, and 4 corresponds to the four sensor data channels: motor angle, HRIF, FMG and sEMG). The input of the LSTM should be a sequence, so each row of the matrix is treated as a frame so that the data matrix is divided into four frames as the input of the LSTM. The network layer of LSTM is shown in Figure 10.

IV Experiment Protocol

Four healthy subjects (two males and two females, 20 ~ 30 years old) without any history of neuromuscular disorder were recruited. Before the experiments, all participants provided written informed consent, and all the experimental protocols were approved by the Institutional Review Board in the Faculty of Engineering, Kagawa University (Ref. No. 01-011), which follows the ethical principle of the Declaration of Helsinki.

In the telerehabilitation platform, one human operator (serves as the therapist) operates the handle of the HD^2 haptic device (the therapist-side robot in the implemented telerehabilitation platform). The motion signals are transmitted to the slave side through the cloud server to control the exoskeleton to assist the patient's movement. The experimental setup is shown in Figure 11. The HRIF between the patient's affected limb and the rehabilitation exoskeleton robot is transmitted from the slave side to the master side, and then the physician can intuitively feel the interaction force. At the same time, the motion angles, the HRIF, sEMG and FMG signals of the patient's affected side are recorded. For each subject, five experimental trials are performed, and each experiment is conducted for 60 seconds.

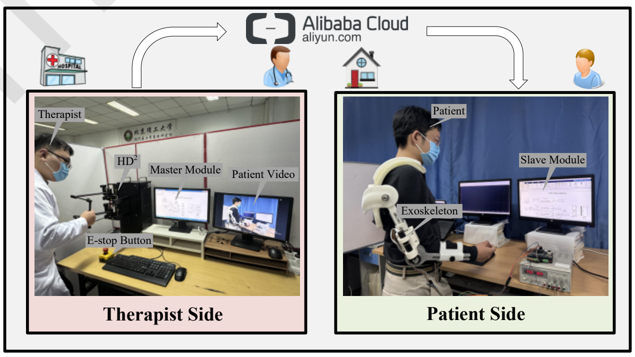

Figure 11. The experimental setup.

There are two conditions during the above experiments. Condition 1 is conducted on patients with complete hemiplegia (healthy people simulate this condition with passive movements). In this condition, the participant is in a completely relaxed state, and the movement of the affected side is completely driven by the upper limb rehabilitation exoskeleton. Condition 2 is conducted on people with active movements. In this condition, the affected side of the participant moves with the movement of the upper limb exoskeleton, that is, the movements of the affected side are active rather than completely driven by the exoskeleton.

Since this study is carried out on healthy subjects, they could not simulate multiple rehabilitation stages, so two extreme cases are performed, as mentioned above: (1) complete hemiplegia - with passive movements ($X_{passive}$) and (2) no hemiplegia - with active movements (X_{active}). Further considering that the classification of the two conditions is too simple, the data are derived into four categories by a heuristic linear interpolation method. Intermediate states ("severe hemiplegia X_{pp}" and "mild hemiplegia X_{pa}") were synthesized by applying predefined proportional coefficients to these baseline signals. Specifically, the coefficient set (0.7, 0.3) was chosen heuristically to represent a gradual shift in the dominance from robot assistance to patient volition. The synthesized data for the intermediate states were generated according to the following equations:

$$X_{pp} = 0.7X_{passive} + 0.3X_{active} \tag{11}$$

$$X_{pa} = 0.7X_{active} + 0.3X_{passive} \tag{12}$$

In summary, the state of motion can be categorized into the following four types: (1) complete hemiplegia, (2) severe hemiplegia, (3) mild hemiplegia, and (4) no hemiplegia. The workflow of data fusion is presented in Figure 12, including data preparation, preprocessing, data derivation, and evaluation based on the BPNN model.

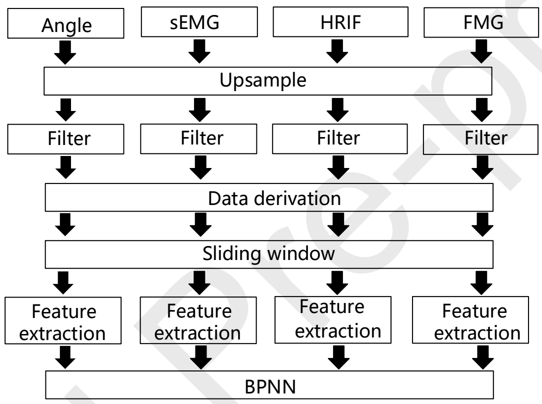

Figure 12. The workflow of data fusion

V Results and Discussion

A. Master-Slave Position Tracking

During the telerehabilitation, the direct kinesthetic supervision of the therapist can be delivered to the stroke patient. The HRIF can also be perceived by the therapist. Figure 13(a) shows the motion trajectory over time. The blue line represents the motion signal on the therapist side, and the orange line represents the motion signal on the patient side. Figure 13(b) shows the contact force between the affected limb and the exoskeleton robot.

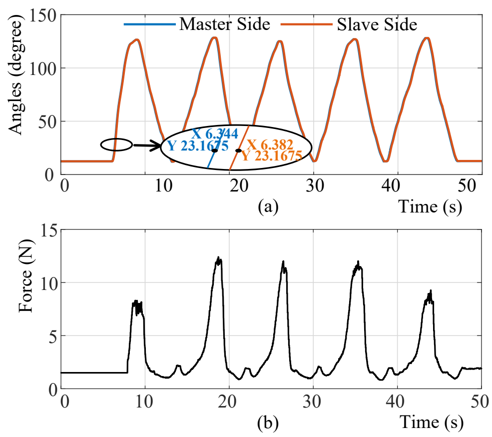

Figure 13 Motion angles and HRIF, (a) Motion angles of master side and slave side, (b) HRIF in the

slave side.

For the quantitative analysis of the communication delay between master side and slave side, the time delay is recorded in TABLE I. The maximum time delay is 54.80 ms, the minimum time delay is 25.20 ms, and the average time delay is 38.43 ms.

TABLE I. The Time Delay of Data Transmission between Master Side and Slave Side

	Time Delay (ms)
MIN	25.20
MAX	54.80
Ave	38.43

For the quantitative analysis of the master-slave position tracking error, MAE, RMSE, and R are adopted for evaluation, as recorded in TABLE II. Taking MAE as an example, the maximum tracking error is 1.4294 degrees, the minimum is 0.6782 degrees, and the average is 0.9989 degrees.

TABLE II. The Tracking Effect between Master Side and Slave Side

Index		Value
MAE	MIN	0.6782
	MAX	1.4294
	Ave	0.9989
RMSE	MIN	0.8404
	MAX	1.7702
	Ave	1.2750
R	MIN	0.9989
	MAX	0.9998
	Ave	0.9994

B. Raw Data of Multi-sensor Signals

This section presents the experimental results and analyses. The raw data are shown in Figure 14, (a)-(d) correspond to complete hemiplegia, (e)-(h) corresponds to no hemiplegia. Figure 14(a)(e) plot the motion angles, (b)(f) plot the HRIF signals, (c)(g) plot the FMG signals, (d)(h) plot sEMG signals. Through Figure 14, it can be observed that in the state of complete hemiplegia, the corresponding HRIF is large, the muscle force is weak, and the sEMG signal has no obvious regularity. In the state of no hemiplegia, the corresponding HRIF is small, the muscle force is stronger, and the sEMG signal has obvious correspondence with the continuous movements of the upper limb.

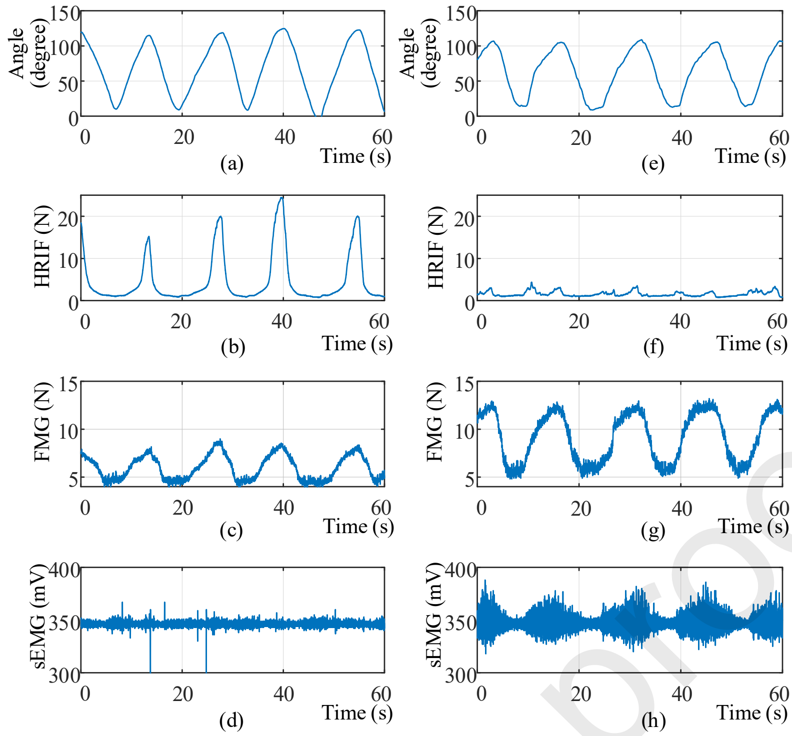

Figure 14. Raw data of multi-sensor, (a)-(d) with passive movements, (e)-(h) with active movements. (a)(e) motion angle, (b)(f) HRIF, (c)(g) FMG, (d)(h) sEMG

C. Motion Angle - Fusion

For motion angles, they are closely related to the strength of sEMG and FMG signals, that is, the greater the maximum angle of elbow flexion, the greater the peak value of sEMG and FMG signals. Here, a small comparison is made concerning whether motion angles are integrated, and the results are recorded in TABLE III. It can be seen from the table that the classification accuracy is improved for both single-sensor and multi-sensor configurations when the motion angles are added. In particular, the motion angle plays a significant role in improving the classification accuracy based on HRIF and FMG. Therefore, motion angle is also considered in the multi-sensor fusion process.

TABLE III. COMPARISON RESULTS WITHOUT AND WITH FUSION OF MOTION ANGLES

Condition	**Without (%)**	**With (%)**
HRIF	78.8179	93.2978
FMG	77.2591	96.1487
sEMG	94.3398	97.6992
HRIF + FMG + sEMG	99.5915	99.6666

D. Comparison of Different Machine Learning Algorithms

To demonstrate the effectiveness of multi-sensor fusion, four kinds of machine learning algorithms are used to compare the classification results before and after fusion. The four machine learning algorithms are Decision Tree (DT), Naive Bayes (NB), Support Vector Machine (SVM) and BPNN, as shown in TABLE IV. The results are for the four classifications of the derived data. This table shows the classification results based on a single sensor, as well as the classification results of two-sensor fusion and three-sensor fusion (except motion angle). Compared with other machine learning algorithms, BPNN has the highest classification accuracy. Further, the classification accuracy based on the three-sensor fusion is the highest, which demonstrates the effectiveness of multi-sensor fusion in rehabilitation assessment.

TABLE IV. COMPARISON RESULTS WITH MULTI-SENSOR INFORMATION FUSION UNDER DIFFERENT MACHINE LEARNING ALGORITHMS

Subject	**Method**	**Condition (%)**

		HRIF	FMG	sEMG	HRIF + FMG	HRIF + sEMG	FMG + sEMG	HRIF + FMG + sEMG
S1	**DT**	53.0	57.3	77.3	68.6	79.4	81.3	84.1
	NB	28.8	29.9	59.7	38.3	60.4	63.5	63.9
	SVM	60.9	64.4	80.1	83.7	85.9	90.7	94.0
	BPNN	61.7	65.4	80.5	84.8	87.4	91.9	**95.8**
S2	**DT**	60.7	65.6	69.5	76.5	78.2	78.0	84.6
	NB	37.3	46.3	50.0	48.0	53.3	52.2	55.5
	SVM	63.9	67.8	74.0	85.3	85.0	85.1	92.6
	BPNN	65.9	68.0	74.3	86.1	86.8	85.9	**94.9**
S3	**DT**	68.9	82.2	69.3	91.9	83.7	85.6	92.3
	NB	41.8	50.9	51.7	52.8	57.0	60.4	65.4
	SVM	69.1	82.1	69.6	94.0	85.3	87.3	95.0
	BPNN	71.6	84.0	72.9	97.1	90.8	92.0	**98.6**
S4	**DT**	53.2	58.9	62.0	68.8	66.3	75.9	79.6
	NB	35.2	36.8	46.4	46.4	48.4	50.1	52.0
	SVM	54.4	62.9	63.1	77.5	76.2	85.0	90.0
	BPNN	55.6	65.4	67.5	81.4	78.2	87.2	**93.3**

To have a more intuitive comparison, Figure 15 plots the comparison histogram under BPNN. It can be found from this figure that the classification accuracy is the highest with the multi-sensor fusion for all subjects. It can be found that individual differences are large. For the 1st subject (S1), the classification accuracy based on sEMG is much higher than those based on the other two sensors. For the 3rd subject (S3), the classification accuracy based on FMG is much higher than those based on the other two sensors. For the 2nd subject (S2), the classification accuracies based on three sensors are not substantially different. For the 4th subject (S4), the classification accuracy based on HRIF is much lower than those based on the other two sensors. Further to intuitively observe the overall effect of classification on each category, the model using a classification confusion matrix is analyzed, as shown in Figure 16, (a)-(d) correspond to the four subjects in turn. For S1 and S2, the classification error is highest for category 1 (severe hemiplegia). For S3, the classification error is highest for category 2 (mild hemiplegia). For S4, the classification error is highest for category 4 (no hemiplegia). No matter for which subject, the classification accuracy of each category is more than 90%.

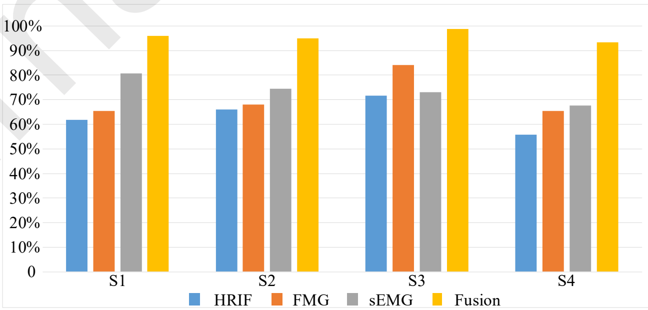

Figure 15. The comparison histogram under BPNN

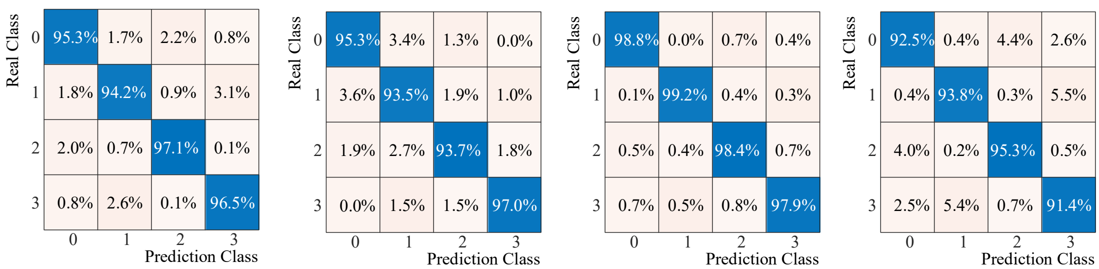

(a) (b) (c) (d)

Figure 16. Confusion matrix of different subjects under BPNN (a) S1 (b) S2 (c) S3 (a) S4

Considering that the collected signals are time series, LSTM is further adopted. The comparison of prediction results under BPNN and LSTM is recorded in TABLE V. Compared with BPNN, LSTM further improves the classification accuracy, with each subject achieving above 95%. These results demonstrate the advantages of LSTM in multi-temporal signal fusion.

TABLE V. COMPARISON OF PREDICTION RESULTS UNDER BPNN AND LSTM

Subject	BPNN (%)	LSTM (%)
S1	96.0	98.2
S2	94.9	96.4
S3	98.6	98.9
S4	93.3	95.9

As rehabilitation robots for patients with hemiplegia gradually enter clinical application, there is still no effective conclusion on the corresponding relationship between assessment methods and robot training parameters that can be applied clinically so far. Therefore, the assessment methods should be taken into account in the development of multidisciplinary rehabilitation robots. This study serves as a proof-of-concept conducted with healthy subjects simulating impaired movement. A primary limitation is that these simulations cannot fully replicate the complex neuromuscular responses of actual stroke patients, such as spasticity or involuntary synergistic movements. Consequently, the performance of the assessment model and the system's response to intense patient-robot interaction in clinical settings remain to be validated. However, the integrated HRIF sensing channel is explicitly designed to capture such high-impedance events, forming the basis for future development of adaptive safety strategies. The immediate next step is to improve the system and further conduct pilot trials with clinical patients to refine the assessment method, establish patient-specific benchmarks, and evaluate the entire telerehabilitation system's efficacy and safety in a real-world therapeutic context.

VI CONCLUSION

In this study, an assessment method of exoskeleton-assisted upper limb rehabilitation using multi-sensor fusion is proposed. The experiments are carried out for the two conditions of passive and active movements, corresponding to patients with complete hemiplegia and healthy subjects without hemiplegia respectively. Further, four rehabilitation states are derived from the preprocessed data, namely complete hemiplegia, severe hemiplegia, mild hemiplegia, and no hemiplegia. Finally, the classification of the four rehabilitation states is accomplished based on the multi-sensor fusion data. The proposed objective assessment method has the potential to help therapists better grasp the rehabilitation process of patients and design more appropriate rehabilitation training programs.

FUNDING

This work was supported by the Tianjin Municipal Education Commission Scientific Research Program (No. 2025ZD048).

ACKNOWLEDGMENTS

The authors would like to acknowledge all the subjects for participating in this research.

REFERENCES

[1] C. W. Tsao, A. W. Aday, Z. I. Almarzooq, et al., "Heart Disease and Stroke Statistics-2023 Update: A Report From the American Heart Association," Circulation, vol. 147, no. 8, pp. e93-e621, Feb. 2023, doi: 10.1161/cir.0000000000001123.

[2] F. Xiong, X. Liao, J. Xiao, et al., "Emerging Limb Rehabilitation Therapy after Post-stroke Motor Recovery," Front. Aging Neurosci., vol. 23, no. 14, Mar. 2022, Art. no. 863379, doi: 10.3389/fnagi.2022.863379.

[3] C. Stinear, C. Lang, S. Zeiler and W. Byblow, "Advances and challenges in stroke rehabilitation," Lancet Neurol., vol. 19, no. 4, pp. 348-360, Apr. 2022, doi: 10.1016/s1474-4422(19)30415-6.

[4] Y. Liu, S. Guo, Z. Yang, H. Hirata and T. Tamiya, "A Home-based Tele-rehabilitation System With Enhanced Therapist-patient Remote Interaction: A Feasibility Study," IEEE J. Biomed. Health. Inform., vol. 26, no. 8, pp. 4176-4186, Aug. 2022, doi: 10.1109/JBHI.2022.3176276.
[5] H. Li, S. Guo, D. Bu, H. Wang and M. Kawanishi, "Subject-Independent Estimation of Continuous Movements Using CNN-LSTM for a Home-Based Upper Limb Rehabilitation System," IEEE Robot. Autom. Lett., vol. 8, no. 10, pp. 6403-6410, Oct. 2023, doi: 10.1109/LRA.2023.3303701.
[6] Y. Liu, S. Guo, Z. Yang, H. Hirata and T. Tamiya, "A Home-Based Bilateral Rehabilitation System With sEMG-based Real-Time Variable Stiffness," IEEE J. Biomed. Health. Inform., vol. 25, no. 5, pp. 1529-1541, May 2021, doi: 10.1109/JBHI.2020.3027303.
[7] E. Zasadzka et al., "Application of an EMG-Rehabilitation Robot in Patients with Post-Coronavirus Fatigue Syndrome (COVID-19)-A Feasibility Study," Int. J. Environ. Res. Public Health., vol. 19, no. 16, Jun. 2022, Art. no. 10398, doi: 10.3390/ijerph191610398.
[8] C. Lambelet, M. Lyu, D. Woolley, R. Gassert and N. Wenderoth, "The eWrist — A wearable wrist exoskeleton with sEMG-based force control for stroke rehabilitation," 2017 International Conference on Rehabilitation Robotics (ICORR), London, UK, Jul. 2017, pp. 726-733, doi: 10.1109/ICORR.2017.8009334.
[9] C. Lambelet, M. Wirth, D. G. Woolley, et al., "Characterization and wearability evaluation of a fully portable wrist exoskeleton for unsupervised training after stroke", J. Neuroeng. Rehabilitation, vol. 17, no. 1, Oct. 2020, Art. no. 132, doi: 10.1186/s12984-020-00749-4.
[10] D. Shi, W. Zhang and X. Ding, "A Review on Lower Limb Rehabilitation Exoskeleton Robots," Chin. J. Mech. Eng., vol. 32, no. 74, Aug. 2019, Art. no. 2019, doi: 10.1186/s10033-019-0389-8.
[11] K. Liu, M. Yin and Z. Cai, "Research and application advances in rehabilitation assessment of stroke," J. Zhejiang Univ. Sci. B., vol.23, no.8, pp.625–641, Aug. 2022, doi: 10.1631/jzus.B2100999.
[12] A. Basteris, S.M. Nijenhuis, A.H. Stienen, et al., "Training modalities in robot-mediated upper limb rehabilitation in stroke: a framework for classification based on a systematic review," J NeuroEngineering Rehabil., vol. 11, Jul. 2014, Art. no. 111, doi: 10.1186/1743-0003-11-111.
[13] R. Zhang, X. Li, Y. Wang, et al., "Using Brain Network Features to Increase the Classification Accuracy of MI-BCI Inefficiency Subject," IEEE Access, vol.7, pp.74490-74499, May 2019, doi: 10.1109/ACCESS.2019.2917327.
[14] J. Bai and A. Song, "Development of a Novel Home Based Multi-Scene Upper Limb Rehabilitation Training and Evaluation System for Post-Stroke Patients," IEEE ACCESS, vol.7, pp. 9667-9677, Jan., 2019, doi: 10.1109/ACCESS.2019.2891606.
[15] L. Lu et al., "Evaluating rehabilitation progress using motion features identified by machine learning," IEEE Trans. Biomed. Eng., vol. 68, no. 4, pp. 1417–1428, Apr. 2021, doi: 10.1109/TBME.2020.3036095.
[16] F. Grimm, J. Kraugmann, G. Naros, and A. Gharabaghi, "Clinical validation of kinematic assessments of post-stroke upper limb movements with a multi-joint arm exoskeleton," J. NeuroEng. Rehabil., vol. 18, no. 1, pp. 1–11, Dec. 2021, doi: 10.1186/s12984-021-00875-7.
[17] K. Ding, B. C. Zhang, Z. Q. Ling, et al., "Quantitative evaluation system of wrist motor function for stroke patients based on force feedback," Sensors, vol. 22, no. 9, p. 3368, Apr. 2022, doi: 10.3390/s22093368.
[18] H. R. Zhao, J. G. Kou, Q. Guo, et al., "Multilevel Control Strategy of Human–Exoskeleton Cooperative Motion With Multimodal Wearable Training Evaluation," IEEE Trans. Control Syst. Technol., vol. 33, no. 2, pp. 434 - 448, Mar. 2025, doi: 10.1109/TCST.2024.3477299.
[19] J. G. Kou, Y. X. Wang, Z. L. Chen, et al., "Gait Planning and Multimodal Human-Exoskeleton Cooperative Control Based on Central Pattern Generator," IEEE-ASME Trans. Mechatron., vol. 30, no. 4, pp. 2598 – 2608, Aug. 2025, doi: 10.1109/TMECH.2024.3453037.
[20] Z. G. Xiao and C. Menon, "A review of force myography research and development," Sensors, vol. 19, no. 20, Oct. 2019, Art. no. 4557, doi: 10.3390/s19204557.
[21] C. Ahmadizadeh, L. Merhi, B. Pousett, et al., "Toward intuitive prosthetic control: solving common issues using force myography, surface electromyography, and pattern recognition in a pilot case study," IEEE Robot Autom. Mag., vol. 24, no. 4, pp. 102-111, Dec. 2017, doi: 10.1109/MRA.2017.2747899.
[22] Y. Zhao, Z. Zhang, Z. Li, et al., "Dehghani-Sanij and S. Xie, "An EMG-Driven Musculoskeletal Model for Estimating Continuous Wrist Motion," IEEE Trans. Neural Syst. Rehabilitation Eng., vol. 28, no. 12, pp. 3113-3120, Dec. 2020, doi: 10.1109/TNSRE.2020.3038051.
[23] Z. H. Cao, D. S. Gao, S. Q. Li, "Application of surface electromyography in upper limb rehabilitation after stroke," Adv. Clin. Exp. Med., vol. 14, no. 2, pp. 2982-2987, Feb. 2024, doi: 10.12677/acm.2024.142422.

[24] Z. Yang, S. Guo, Y. Liu, et al. “An intention-based online bilateral training system for upper limb motor rehabilitation,” Microsyst. Technol., vol. 27, pp. 211–222, Jan. 2021, doi: 10.1007/s00542-020-04939-x.
[25] H. Li, S. Guo, D. Bu and H. Wang, “Inter-subject Variability Evaluation of Continuous Elbow Angle from sEMG using BPNN,” 2022 IEEE International Conference on Mechatronics and Automation (ICMA), Guilin, Guangxi, China, Aug. 2022, pp. 388-393, doi: 10.1109/ICMA54519.2022.9856005.
[26] H. Li, S. Guo, H. Wang and D. Bu, “Subject-Independent Continuous Estimation of sEMG-Based Joint Angles Using Both Multisource Domain Adaptation and BP Neural Network,” IEEE T. Instrum. Meas., vol. 72, pp. 1-10, Nov. 2022, Art no. 4000910, doi: 10.1109/TIM.2022.3225015.

Highlights

- This paper builds an exoskeleton-assisted upper limb telerehabilitation system with the help of cloud server.
- Based on the telerehabilitation system, an assessment method using multi-sensor information fusion is proposed.
- The experiments are conducted with passive movements and active movements.
- It has the potential to promote the assessment methods that are compatible with rehabilitation training exoskeleton robots.

Declaration of interests

☒ The authors declare that they have no known competing financial interests or personal relationships that could have appeared to influence the work reported in this paper.

☐ The authors declare the following financial interests/personal relationships which may be considered as potential competing interests:

ACKNOWLEDGMENT

The authors would like to acknowledge all the subjects for participating in this research.